

This is an Open Access document downloaded from ORCA, Cardiff University's institutional repository: <https://orca.cardiff.ac.uk/id/eprint/141826/>

This is the author's version of a work that was submitted to / accepted for publication.

Citation for final published version:

Junqueira, Adriano M., Mao, Feng , Mendes, Tatiana S. G., Simões, Silvio J. C., Balestieri, José A. P. and Hannah, David M. 2021. Estimation of river flow using CubeSats remote sensing. *Science of the Total Environment* 788 , 147762. 10.1016/j.scitotenv.2021.147762

Publishers page: <http://dx.doi.org/10.1016/j.scitotenv.2021.147762>

Please note:

Changes made as a result of publishing processes such as copy-editing, formatting and page numbers may not be reflected in this version. For the definitive version of this publication, please refer to the published source. You are advised to consult the publisher's version if you wish to cite this paper.

This version is being made available in accordance with publisher policies. See <http://orca.cf.ac.uk/policies.html> for usage policies. Copyright and moral rights for publications made available in ORCA are retained by the copyright holders.



1 Estimation of river flow using CubeSats remote sensing

2
3 Adriano M. Junqueira ^{a,b*}, Feng Mao ^c, Tatiana S. G. Mendes ^d, Silvio J. C. Simões ^{a,c},

4 José A. P. Balestieri ^a, David M. Hannah ^b

5 ^a São Paulo State University (UNESP), School of Engineering, Guaratinguetá - Brazil

6 ^b University of Birmingham, School of Geography, Earth and Environmental Sciences, Birmingham –

7 United Kingdom

8 ^c Cardiff University, School of Earth and Environmental Sciences, Cardiff - United Kingdom

9 ^d São Paulo State University (UNESP), Institute of Science and Technology, São José dos Campos - Brazil

10 *Corresponding author:

11 Email: adriano.junqueira@unesp.br (A. M. Junqueira)

12 Av. Dr. Ariberto Pereira da Cunha, 333 – Guaratinguetá – SP – Brazil – Zipcode: 12516-410

14 **Abstract:**

15
16 River flow characterizes the integrated response from watersheds, so it is essential to quantify to
17 understand the changing water cycle and underpin the sustainable management of freshwaters.
18 However, river gauging stations are in decline with ground-based observation networks shrinking.
19 This study proposes a novel approach of estimating river flows using the Planet CubeSats
20 constellation with the possibility to monitor on a daily basis at the sub-catchment scale through
21 remote sensing. The methodology relates the river discharge to the water area that is extracted
22 from the satellite image analysis. As a testbed, a series of Surface Reflectance PlanetScope images
23 and observed streamflow data in Araguaia River (Brazil) were selected to develop and validate
24 the methodology. The study involved the following steps: (1) survey of measurements of water
25 level and river discharge using in-situ data from gauge-based Conventional Station (CS) and
26 measurements of altimetry using remote data from JASON-2 Virtual Station (JVS); (2) survey of
27 Planet CubeSat images for dates in step 1 and without cloud cover; (3) image preparation
28 including clipping based on different buffer areas and calculation of the Normalized Difference

29 Vegetation Index (NDVI) per image; (4) water bodies areas calculation inside buffers in the Planet
30 CubeSat images; and (5) correlation analysis of CubeSat water bodies areas with JVS and CS
31 data. Significant correlations between the water bodies areas with JVS ($R^2 = 88.83\%$) and CS (R^2
32 $= 96.49\%$) were found, indicating that CubeSat images can be used as a CubeSat Virtual Station
33 (CVS) to estimate the river flow. This newly proposed methodology using CubeSats allows for
34 more accurate results than the JVS-based method used by the Brazilian National Water Agency
35 (ANA) at present. Moreover, CVS requires small areas of remote sensing data to estimate with
36 high accuracy the river flow and the height variation of the water in different timeframes. This
37 method can be used to monitor sub-basin scale discharge and to improve water management,
38 particularly in developing countries where the presence of conventional stations is often very
39 limited.

40

41 **Highlights:**

42

- 43 • Use of remote sensing information from Planet CubeSats constellation to build and assess a
44 methodology to river flow estimation;
- 45 • This method has significant opportunity for river flow estimation at ungauged sites at the daily
46 and sub-basin scales;
- 47 • The improvement of river flow measurements is essential to understand the changing water
48 cycle and underpin the sustainable management of freshwaters.

49

50 **Keywords:** River flow; CubeSat; Remote Sensing; Cerrado (Savannah); Change Detection;
51 Spatiotemporal Resolution.

52

53

54 **1 Introduction**

55

56 Freshwater is a basic requirement for life but the knowledge of river flow rates is scarce
57 (Gleason and Smith, 2014). A better understanding of the large-scale water cycle process is
58 essential to underpin socio-economic development and sustainably manage water-dependent
59 ecosystems (Döll et al., 2014; Hannah et al., 2011; Kingston et al., 2020). River flow characterizes
60 the integrated hydrological response and water yield from watersheds. Nowadays, there is a clear
61 decline of river gauging stations and a shrinking of ground-based observation networks (Dixon et
62 al., 2020; Hannah et al., 2011).

63 Conventional gauging stations are well developed and have contributed to quantify the
64 movement of water in river channels. However, conventional stations are not enough to determine
65 more complex riverine environments that involve the movement of water over wetlands and
66 floodplains in multiple channel types (Lettenmaier, 2007), requiring new multidisciplinary
67 approaches to improve the observation networks.

68 The advances in remote sensing hydrology, particularly over the past 10 years, have
69 demonstrated that hydraulic variables can be measured reliably from orbiting satellite platforms
70 (Huang et al., 2018). As the deluge of big data continues to impact practically every commercial
71 and scientific domain, geosciences have also witnessed a major revolution from being a data-poor
72 field to a data-rich field (Karpatne et al., 2019; Reichstein et al., 2019). The use of remote sensing
73 by satellite for streamflow analyses can be categorized into techniques based on satellite altimetry,
74 Synthetic Aperture Radar (SAR), and optical images (Ahmad and Kim, 2019).

75 To accurately detect river flow regimes at a field scale from space, a new high spatial and
76 temporal resolution remote sensing source is necessary to improve water-level time series
77 (Bogning et al., 2018). While satellites such as Sentinel-2 and Landsat may have an adequate
78 spatial resolution for different applications (Sadeh et al., 2019), their temporal resolution (5 and
79 16 days revisit time, respectively) is not ideal for detection of flow regimes changes, as there may
80 be weeks between the acquisition of two clear-sky images (Houborg and McCabe, 2018a).

81 Applications of satellite remote sensing in hydrological surface water modelling, mapping,
82 and parameter estimation were reported in some reviews based on Earth Observing Systems
83 (Huang et al., 2018; Joshi et al., 2016; Musa et al., 2015; Wagner et al., 2018) mainly using SAR,
84 optical, altimetry and DEM data. Focusing flow river estimation, different techniques were
85 applied to estimate the river width by averaging multiple cross-sections over an area (Gleason
86 and Smith, 2014), use the Synthetic Aperture Radar (SAR) to calculate water area (Ahmad and
87 Kim, 2019), and fusion topography dataset (Anh and Aires, 2019; Moramarco et al., 2019). The
88 spatiotemporal restrictions for using remote sensing satellite data have been partly overcome via
89 multisensor data fusion (Houborg and McCabe, 2018b) but all solutions proposed can not be
90 replicated for daily measurements at a high spatial resolution.

91 Thus, remote sensing has the potential of conducting rapid, cost-effective, and continuous
92 surveys of river management practices over large scales. Notably, the constellations of micro or
93 nano-satellites, known as CubeSats, are revolutionizing the high spatiotemporal resolution
94 possibilities in remote sensing and can potentially be used to capture many observations over time
95 (Sadeh et al., 2019) and monitor dynamics surface water changes (Cooley et al., 2019, 2017). The
96 repetitive observation mechanism of multiples CubeSats enables studying the river dynamics and
97 observe different physical properties (Marinho et al., 2020). Among the different Cubesats on orbit,
98 the CubeSat constellation provided by Planet Labs Inc. has the advantage of providing a near-
99 daily revisit time globally at 3-meter orthorectified spatial resolution. It is also worth noting that
100 Remote Sensing (RS) has several methods and techniques to identify land and water areas
101 considering bands variation of different multi-spectral images (Acharya et al., 2018). Index
102 methods are mostly used to estimate surface water that separates the water from the background
103 based on a threshold value. Among these indexes, Normalized Difference Vegetation Index
104 (NDVI) and Normalized Difference Water Index (NDWI) are frequently adopted as they include
105 visible and Near Infrared (NIR) bands provided by satellite optical images (Elsahabi et al., 2016).

106 The aims of this study were (1) to develop an innovative methodology for semi-automated
107 river flow estimation using visible and NIR from Planet CubeSats bands to detect changes in the
108 surface of flood area and (2) to compare Planet CubeSats derived river flow with Conventional

109 flow meters Station (CS) and JASON (Joint Altimetry Satellite Oceanography Network) Virtual
110 gauging Station (JVS). The Araguaia River, in the Cerrado biome of Brazil, was selected as the
111 research area.

112

113 **2. Description of the study area**

114

115 The Tocantins-Araguaia hydrographic region, with a total area of 920,087 km² and 13,779
116 m³/s of average discharge (Brasil/ANA, 2015), is the most important fluvial system draining the
117 tropical savannah ecoregion of Brazil (Cerrado biome). Some areas of this region have been
118 affected by severe water scarcity events since 2012 (Naturatins, 2017). In general terms, the
119 hydrologic regime depends on the dominant climate (tropical wet-dry) with floods from January
120 to May (rain period) and low water between June to September. This region is the confluence of
121 two major rivers: the Tocantins River (~1,960 km extension) and the Araguaia River (~2,600 km
122 extension). The Araguaia sub-basin (around 386,765 km²) represents around 42% of the
123 hydrographic region and along its path, is placed the largest river island in the world, Bananal
124 Island (Figure 1).

125

126

Figure 1

127

128 The Araguaia River is one of the priority areas for conservation of the aquatic biodiversity of
129 the Cerrado biome and has been the target of political and environmental debates due to the
130 intense and indiscriminate expansion of agricultural activities, with a greater degradation of the
131 natural environment during the last four decades (Latrubesse and Stevaux, 2006). The entire sub-
132 basin has just 166 conventional river gauging stations for an area of 386,765 km² and more than
133 6,000 river stretches mapped.

134 This region needs to be better monitored due to the increase in intensive agriculture and the
135 use of water (Althoff et al., 2020). Especially in the Araguaia River, the irrigated area increased

136 more than 116% between 2006 and 2012, and the cultivated area increased by about 20% in the
137 same period (ANA, 2015). In the last decade, the Araguaia sub-basin has been suffering from
138 water scarcity in several tributaries of the Araguaia river, obliging managers to take actions for
139 rationing the water use in agriculture to prioritize human and animal supply (Lauris, 2019;
140 Naturatins, 2017).

141 As a testbed to develop and validate the proposed methodology, two river gauging stations
142 that are calibrated by ANA and used as an official instrument for public policies in this region
143 were selected. One of the rivers gauging stations was the in-situ Conventional Station (CS) ID
144 26350000 (<http://gestorpcd.ana.gov.br>) managed by ANA, located in São Felix do Araguaia –
145 MT (11°37'8.6" S; 50°39'75.0" W – WGS84 Datum). This station employs an instrument for
146 monitoring the river flow for 24/7 hours with records registered every 15 minutes. The other river
147 gauging station was the JASON-2 Virtual Station (JVS) ID 1055S05036WO
148 (<http://hidrosat.ana.gov.br>), which is monitored by ANA in cooperation with Institut de
149 Recherche pour le Développement (IRD) with barycenter data at 10°54'42.0" S; 50°36'48.6" W
150 – WGS84 Datum. This station acquires altimetry information by satellite to monitor the water
151 level and derived river flow, with no equipment locally installed. The JVS dataset is related to the
152 average altitude of all available altimetry data, along the JASON-2 track, over the river area in
153 each satellite cycle. JVS observations occur every 9.9 days from the JASON-2 satellite in the
154 same ground track within a margin of ± 1 km (CNES; NASA, 2011).

155 The detailed characteristics of both selected stations are shown in Figure 2. The distance
156 between the CS and JVS is relatively close with 78 km (Euclidean distance) allowing their
157 comparison with the proposed methodology.

158

159

Figure 2

160

161

3. Data and Methods

For this study, the available Planet CubeSat data was explored to establish an innovative method for estimating river flow based on daily remote sensing images.

3.1. CubeSat data

This study used Planet images to develop a flow estimation model. These images are captured by Planet using an approach based on ‘fast design’ to launch satellites, mission control and operations systems, and the development of a web-based platform for imagery processing and delivery (www.planet.com). Planet is a commercial satellite operator that enhanced observation capacity offered by constellations of small and standardized satellites and employs an “always-on” image-capturing method (Planet Team, 2020).

This CubeSat constellation consists of 130 small-satellites at an altitude of approximately 475 km, following each other on two near-polar orbits of roughly 8° (descendent orbit) and 98° (ascendent orbit) inclination respectively, imaging the Earth at local morning time (Planet Team, 2020). The distance along the orbit between the CubeSats is constructed such that the longitudinal progression between them over the rotating Earth leads to the scan of the surface. Thus, the full constellation provides daily sun-synchronous coverage of the entire Earth (except the polar hole) with the resolution of 3.7 meters at nadir (Ground Sample Distance), 12-bit radiometric resolution, and 4 spectral bands (Blue [455 - 515 nm], Green [500 - 590 nm], Red [590 - 670 nm] and Near-InfraRed [780 - 860 nm]) (Planet Team, 2020).

The CubeSat across-track off-nadir viewing angle used for imaging usually to be lower than 5° (Planet Team, 2020) reducing the complexity to evaluate bands’ variation of different multi-spectral images arising from environmental noise such as shadow, however, these CubeSat do not present any spectral bands as Middle Infrared (MIR) and Shortwave Infrared (SWIR), used in different indexes applied to water such as TCW, MNDWI, NDWI, AWEI (Elsahabi et al., 2016).

189 The images can be downloaded from the Planet portal (<https://www.planet.com/explorer>) and
190 include three types of raster images: (a) digital number (DN) commonly represented by an
191 uncalibrated image into physically meaningful units; (b) top of atmosphere reflectance (TOA)
192 that is the reflectance measured by a space-based sensor flying higher than the earth's atmosphere
193 (calibrated to a radiance image), and (c) surface reflectance (SR) that is the radiance image
194 atmospherically corrected and ready to be used to extract quantitative information about features
195 on the Earth surface. As SR reflects the difference among land covers more accurately than other
196 remotely sensed measurements (Huang et al., 2018). In this study, it was used the SR image
197 products, orthorectified with 3 meters spatial resolution, positional accuracy with less than 10-
198 meters Root Mean Square Error (RMSE) suitable for analytic and visual applications.

199

200 *3.2. A method for estimating river flows using CubeSats*

201

202 This study was divided into five steps: (1) survey of measurements of water level and
203 river discharge using in-situ data from gauge-based Conventional Station (CS) and measurements
204 of altimetry using remote data from JASON-2 Virtual Station (JVS); (2) preparation of river
205 section and buffers and survey of CubeSat images for selected dates (correlated with step 1 and
206 without cloud cover); (3) image preparation, including clipping based on different buffer areas
207 followed by NDVI calculation per image, and data processing over CS and JVS stations using
208 Extract-Transform-Load (ETL); (4) water bodies areas calculation inside buffer for river flow
209 estimation in the Planet CubeSat images; and (5) correlation analysis of CubeSat water bodies
210 areas with JVS and CS data (Figure 3).

211

212

Figure 3

213

214 Firstly, the CS and JVS measurements were collected in the period of 01/01/2018 to
215 30/07/2018, a period that historically includes the greatest variation in the flow of this river over
216 the years. The dataset for CS included the water level and river flow every 15 minutes. The JVS

217 were collected altimetry data in repetitive periods of 10 days according to the measures provided
218 by the altimetry missions satellite. The use of JVS data was independent of the time of collection
219 and resulted in a median of 11:03 a.m. local time.

220 In the second step, a cross-section of the river was used as a reference for creating side buffers
221 with 50, 250, 500, and 1000 meters. This cross-section was determined nearby to the JASON's
222 tracking to provide better conditions of comparison between the virtual stations and these buffers
223 sections were created to reduce the satellite image processing area in the water surface calculation.
224 Using the location of these buffers, Planet CubeSat images were searched for all dates with JVS
225 data. The CubeSat images search also included the completed cover of buffer areas, the absence
226 of clouds, and the possibility of using the surface reflectance product (SR) as input (Table 1).

227 In the third step, each image downloaded from the Planet portal was clipped on the buffer
228 areas and processed to calculate the Normalized Difference Vegetation Index (NDVI) with a scale
229 ranging from -1 to 1. The NDVI was calculated using the Red and Near-InfraRed regions of the
230 electromagnetic spectrum with Equation 1 since these satellites do not have yet more specific
231 spectral bands for the development of more sophisticated methods. For each image analyzed, the
232 river flood areas were classified with NDVI values lower than 0.15.

233

$$234 \quad NDVI = \frac{(NIR\ Band - Red\ Band)}{(NIR\ Band + Re\ Band)} \quad (1)$$

235

236 In the fourth step, the water bodies' areas were calculated for all clipped buffers in the dates
237 analyzed, resulting in a temporal table of flooding areas. Then, in the fifth step, we performed the
238 regression curves (exponential, linear, logarithmic, polynomial, power-law, and moving
239 averages) between the water bodies areas for 4 different buffers (50, 250, 500, and 1000 m) and
240 the 3 sets of reference data (JVS - altimetry, CS - water level, CS - flow). After that, 12 different
241 Pearson coefficients (R^2) were determined according to the best-fitted regression curves. The
242 relationship between R^2 and the four buffer areas were analyzed for each set of reference data,

243 determining the equation used to predict the river flow from the CubeSat image flood area, which
244 represented the CubeSat Virtual Station (CVS).

245

246 **4 Results**

247

248 The data collected from CS showed a river flow ranging from 868 to 4,739 m³/s and a water
249 level varying from 328 to 710 cm for the entire monitoring period in the Araguaia basin. A
250 significant relationship between the river flow and the water level measurements ($R^2=1$) was
251 found (Figure 4a). Concerning the JVS data, altimetry values between 177.9 to 181.1 m were
252 observed, with a good correlation to CS water level ($R^2= 0.85$) (Figure 4b).

253

254 *Figure 4*

255

256 In the survey of Planet CubeSat images, 8 image dates were selected with CS and JVS
257 correspondent data, completed cover the buffer areas, absence of clouds, and available surface
258 reflectance product (SR) (Table 1).

259

260 *Table 1*

261

262 In these 8 images, water bodies areas ranging from 39,924 to 54,846 m² for buffer 50 m, from
263 173,313 to 276,984 m² for buffer 250 m, from 320,805 to 557,586 m² for buffer 500 m, and from
264 563,895 to 1,097,469 m² for buffer 1000 m were determined (Table 2). Considering the maximum
265 values of water bodies in each buffer, it was verified that the flood area corresponds to 77.3%,
266 63.9%, 52.5%, and 37.7%, respectively, for the 50 m, 250 m, 500 m, and 1000 m buffer areas.

267

268 *Table 2*

269

270 Based on the water bodies areas determined in each buffer area, the regression models were
271 performed as demonstrated in Figure 5. Due to the obtained data values and its measure of
272 greatness, the river flow equation was adjusted to the power-law regression model, while the
273 water level and altimetry equations were adjusted to linear regression models.

274

275

Figure 5

276

277 Considering the results obtained in the regression models, it was found that the buffer of 500
278 m was the lowest buffer area capable of providing a high Pearson's coefficient that remained
279 stable even with the increase of buffer area (Figure 6). Therefore, the buffer of 500 m was selected
280 to be the CVS and to estimate the river flow.

281

282

Figure 6

283

284 To estimate the river flow (Q_e), water level (L_e) and altimetry (A_e) were determined the
285 Equations 2 ($R^2 = 96.49\%$), 3 ($R^2 = 94.38\%$) and 4 ($R^2 = 88.83\%$) respectively; in which $Af500r$
286 is the flooding area (m^2) in the 500 m buffer.

287

288

$$Q_e = 10^{-1} \cdot Af500r^{2.8737} \quad (2)$$

289

290

$$L_e = 0.0015 \cdot Af500r - 161.56 \quad (3)$$

291

292

$$A_e = 10^{-5} \cdot Af500r + 175.14 \quad (4)$$

293

294 The root mean square error (RMSE) is used as the accuracy estimator (Equation 5), and the
295 standard deviation (SD) is used as the precision estimator (Equation 6). These estimators were
296 determined for river discharge (Q_e), water level (L_e), and altimetry (A_e) are presented in Table 3.

297

298

$$RMSE = \sqrt{\sum_{n=1}^n \frac{(Reference_n - Calculated_n)^2}{n}} \quad (5)$$

299

300

$$SD = \sqrt{\sum_{n=1}^n \frac{[(Reference_n - Calculated_n) - \overline{(Reference_n - Calculated_n)}]^2}{n-1}} \quad (6)$$

301

302

Table 3

303

304

305

In summary, this CVS methodology established for the Araguaia river can be explored to estimate the river flow, water level, and altimetry for other rivers around the world.

306

307

5 Discussion

308

309

310

311

312

313

314

315

Hydrographic data obtained from satellites and other remote sources provide the possibility of broad global coverage for river discharge estimates (Bahadur and Samuels, 2013; Lakshmi, 2004). The advances in computing power and data storage capacity associated with the innovations in the satellite remote sensing area are enabling global monitoring of different variables related to the water cycle (Lettenmaier et al., 2015; Wagner et al., 2018). Nowadays, the increase in the number of Planet CubeSats brings images with more cost-effective and higher spatiotemporal resolutions than other commercial satellites (Houborg and McCabe, 2018b).

316

317

318

319

320

Currently, Planet CubeSat is the only commercial constellation available for capturing daily optical images with high resolution of the entire surface of the Earth. In Brazil, there is a national program (<https://www.gov.br/mj/pt-br/aceso-a-informacao/acoes-e-programas/programa-brasil-mais/>) that provides Planet images with high-resolution (3 m orthorectified per pixel) freely available to governmental institutions throughout the Brazilian territory.

321

322

323

Access to the CubeSat images is an important political and economic decision. The use of satellite information is an economical way of measuring river discharge using in situ gauges stations that are costly to install, maintain, and operate (Zaji et al., 2018). According to U.S.

324 Geological Survey (USGS), the cost for a typical in situ gauge station evolves several costs
325 associated with its activities, which are estimated at 41% for labour staff (field and office), 25%
326 for administrative activities, 10% for building and utilities, 10% for field equipment, 7% for data
327 management and delivery, 5% for vehicles and 2% for travel (Norris, 2010). These percentages
328 can vary according to location and conditions, especially in remote areas where in situ gauges
329 stations require expensive field works (Norris, 2010). Besides reducing costs, the implementation
330 of technology-based remote sensing for river discharge can avoid exposing surveyors to
331 dangerous and reacher inaccessible rivers (Samboko et al., 2020).

332 Monitoring of rivers requires a reliable system, being the water level and the river discharge
333 the two essential parameters in this analysis (Mao et al., 2020, 2019, 2018; Mostafavi, 2018).
334 Besides that, the monitoring requires integrated modelling tools that cover adequate spatial and
335 temporal scales involving mathematical applications (Mannschatz et al., 2015). In this context,
336 an innovative methodology for river flow estimation was developed using Planet CubeSat images
337 to detect changes in the flood area surface, which can be used as a CubeSat Virtual Station (CVS).

338 Although methods of river discharge from the direct measurement of width, depth, and
339 velocity (based on velocity-area method) provides a higher level of accuracy than orbital remote
340 sensing (Bjerklie et al., 2005), the proposed methodology used an approach that relies on
341 identifying of the water surface from morphologic features that are easier to recognize from space.
342 The geomorphic features and structural dynamics related to river discharge as channel type,
343 channel slope, channel roughness, depth, and velocity were assumed associated with the river
344 hydraulic geometries and can be used to develop more robust calibration methods.

345 The CVS data obtained were compared with the measures of water level and river discharge
346 of a Conventional Station (CS) and altimetry of the JASON Virtual Sation (JVS), located in the
347 Araguaia River (Brazil).

348 Analyzing the CS data collected in this study, it was found a complete correlation ($R^2 = 1$)
349 between the measurements of water level and river discharge, indicating that the in-situ reference
350 station used was well-calibrated. It was also observed a high correlation of the CS water level
351 measurements with the JVS altimetry data ($R^2 = 0.85$) confirming that the satellite remote sensing

352 can be a useful tool for river flow estimation. Bogning et al., (2018) also found a good correlation
353 ($R^2 > 0.82$) when in-situ gauge records were compared to altimetry- based water levels from
354 multiple satellites, composed of a network of altimetric virtual station (ENVISAT, SARAL,
355 ERS- 2, Sentinel- 3A, JASON- 2, and JASON- 3 data). This analysis was performed in the
356 Ogooué river basin, located at Gabon, with an annual river discharge of 4,750 m³/s and a
357 hydrologic wet-dry regime similar to the characteristics of this study in the Araguaia River. Smith
358 and Pavelsky, (2008) demonstrated that remotely sensed width variations were well correlated to
359 ground measurements of river discharge ($R^2 = 0.81$) when taken days later and hundreds of
360 kilometres downstream. Gleason and Smith (2014) showed that useful estimates of absolute river
361 discharge may be obtained solely from river width using multiple satellite Landsat images,
362 through a characteristic scaling law named At-Many-station Hydraulic Geometry (AMHG), with
363 no ground-based or a priori information. The AMHG was calculated with the monitoring of large
364 extensions (10 to 13 km) from remote sensing along the river.

365 JVS and Landsat can be employed in the case of lacking river rating curves and cross-
366 sectional geometries, as well as when the water levels or flow rates measurements are missing in
367 situ station historic data. However, the use of JVS and Landsat data in a river hydrodynamics
368 context is limited by data coverage in both time and space, which may be insufficient to capture
369 key spatiotemporal variations in water surface elevation daily (Houborg and McCabe, 2018a).
370 Besides that, JVS can be used only to monitor the level of wider rivers (Huang et al., 2018) that
371 intersect with JASON-2 satellite tracks.

372 In this study, the innovative method using Planet CubeSat images provides a possibility to
373 monitor river narrower than those evaluated by JVS and Landsat due to its higher spatial
374 resolution (Houborg and McCabe, 2018b, 2018a). Also, Planet constellation allows monitoring
375 rivers around the world (Kääb et al., 2019) with more flexibility to establish Virtual Stations
376 concerning JVS that are limited to the track satellite intersections. The fact of use high-resolution
377 Planet CubeSat images, with low acquisition inclination, reduces the effect of shadow and
378 increases the river border identification details. This agrees with Bjerklie et al. (2003), who
379 reinforces that even if the river could always be distinguished from the surrounding landscape,

380 narrower channels would have greater uncertainty in the width estimates due to the relative width
381 concerning the resolution of the sources. The altimetry accuracy for the JVS stations varies with
382 the river width, with better precision the wider the channels (Bjerklie et al., 2018), while for the
383 proposed CVS stations the accuracy in determining the level varies with the flooded area close to
384 the station, with precision dependent on the slope at the edges of the channel, as it reflects in the
385 expansion of the flooded area.

386 For the period of study, 8 images were selected with dates correspondent to CS and JVS
387 reference measures. However, many other Planet CubeSat images were available in the period,
388 with 110 cloud-free SR images against 22 JVS measures, representing at least 5 times more
389 information than JVS data for the Araguaia river. Although many Planet images were available,
390 it was decided to use only the images that allowed the comparison with CS and JVS on the same
391 date.

392 The data from CubeSat images showed a well-correlated estimation with river discharge
393 ($R^2 = 96.49\%$) when small lengths of the river (500 m buffer) were analyzed. This correlation was
394 higher than the JVS data and river discharge correlation ($R^2=85.01\%$) that is one of reference
395 adopted by the ANA in Brazil. The results using CubeSat images were also well correlated with
396 CS water level ($R^2 = 94.38\%$) and JVS altimetry ($R^2 = 88.83\%$) when evaluated the flooding area
397 (m^2). According to Papa et al. (2010), ideally, the goal for discharge data accuracy is within $\pm 5\%$
398 related to the true value, but the community agrees that 15% to 20% accuracy is in general
399 acceptable for discharge measurements.

400 Virtual stations with CubeSat images showed greater accuracy and precision at lower river
401 discharge rates (Fig. 5) whereas JASON virtual stations have greater accuracy and precision for
402 higher river discharge rates (Fig. 4b). This is observed by the fact that in the CVS, a better
403 refinement of the flooded area is possible even with the presence of sandbanks while the JVS
404 presents greater noise in the identification of the altimetry related to these areas. At higher river
405 discharges, we observed that the JVS presented better details of the altimetry, especially when the
406 increase in the level of the river occurred inside the channel without accompanying the expansion
407 of the flooded area.

408 In this study, it was visually observed a refined design of the flooded areas due to the
409 resolution of the CubeSat images. From this observation, an attempt was made to find a
410 relationship between the width of the river and a buffer size that provided less demand of image
411 areas to achieve a high Pearson coefficient. It was observed that a buffer ranging from 0.5 to 1
412 times the average width of the studied river section allowed to reach these results, remaining
413 stable even the value of R^2 . Then, the proposed methodology allows the use of less than 388 km²
414 of images/year for this virtual station, representing an advantage in comparison with the AMGH
415 methodology, which suggests the evaluation of multiple river widths by stretches greater than 10
416 km. Using 3-meter Planet images as reference, Pôssa et al. (2018) observed a slightly increased
417 precision in the water surface delineation compared to Landsat and Sentinel images due to spatial
418 resolution of satellite images.

419 Overall, these experiments allow us to employ a simple exponential equation model with
420 daily CubeSat images for well predict the river flow at a monthly scale, based on the surface
421 hydrological information measured from space as proof of concept and utility of the method. The
422 use of new constellations, new hydrological science methods, and advancements in resolutions
423 (spatial, temporal, and radiometric) of remote sensing make possible the application of monitoring
424 increasingly smaller watersheds, as they have coverage of several pixels and more frequent data
425 acquisitions (Lakshmi, 2004). Besides that, to flow estimation measurement, the CubeSat images
426 can be used to study other processes related to data assimilation; flood monitoring and prediction;
427 floodplain connectivity (Cooley et al., 2017); land surface characteristics (land use, temperature,
428 snow cover) (Reichle, 2008); image fusion to land use mapping and monitoring (Houborg and
429 McCabe, 2018b; Joshi et al., 2016); and water quality monitoring (Maciel et al., 2020).

430

431 **6 Conclusion**

432

433 An innovative method for semi-automated river flow estimation using Planet CubeSat data
434 was developed to detect changes in the surface of the flood area, using the Araguaia River as a
435 testbed. In summary, the flood areas detected by CubeSat data showed significant correlations
436 with river discharge and water level measurements from gauge-based Conventional Station (CS)
437 in small areas of the river using a reduced amount of satellite images. CubeSat data also presented
438 a significant correlation with altimetry measurements from JASON-2 Virtual Station (JVS)
439 officially adopted by the Brazilian agency, with the advantage to provides greater records
440 numbers per year, more flexibility of position for Virtual Stations establishment, and the
441 possibility to monitor narrower rivers. The river discharge extracted from Cubesat data showed a
442 higher correlation with CS than JVS, indicating that CVS had more capacity of reproducing the
443 ground truth compared to JVS.

444 In the future, this method can be completely automated to fill the gaps in the streamflow
445 series, to compute different riverine contributions in the sub-basin, and to promote an
446 understanding of river discharge spatial distribution on a near-real-time for entire continents. This
447 method can also be used as a cost-effective alternative to monitoring the sub-basin discharges,
448 improving water management, particularly, in developing countries where the presence of
449 conventional stations is limited.

450

451 **Acknowledgements**

452

453 The authors are grateful to Brazilian National Water Agency (ANA – Agência Nacional de
454 Águas) for providing the fluvial data in Brazil (conventional and virtual stations) and, to
455 SCCON/PLANET data images accessed from the online portal
456 (<https://www.planet.com/explorer>).

457 This study was financed in part by the Coordenação de Aperfeiçoamento de Pessoal de Nível
458 Superior - Brasil (CAPES) - Finance Code 001.

459 Adriano M. Junqueira was hosted at the University of Birmingham, UK, to undertake this work.
460 Jose Antonio Perrella Balestieri is grateful to the Conselho Nacional de Desenvolvimento
461 Científico e Tecnológico (CNPq), process 301853/2018-5.

462

463 **References**

464

465 Acharya, T.D., Subedi, A., Lee, D.H., 2018. Evaluation of water indices for surface water extraction in a
466 landsat 8 scene of Nepal. *Sensors (Switzerland)* 18, 1–15. <https://doi.org/10.3390/s18082580>

467 Ahmad, W., Kim, D., 2019. Estimation of flow in various sizes of streams using the Sentinel-1 Synthetic
468 Aperture Radar (SAR) data in Han River Basin, Korea. *Int. J. Appl. Earth Obs. Geoinf.* 83, 101930.
469 <https://doi.org/10.1016/j.jag.2019.101930>

470 Althoff, D., Rodrigues, L.N., David, D., 2020. Impacts of climate change on the evaporation and availability
471 of water in small reservoirs in the Brazilian savannah. *Clim. Chang.* 18.

472 Anh, D.T.L., Aires, F., 2019. River discharge estimation based on satellite water extent and topography:
473 An application over the Amazon. *J. Hydrometeorol.* 20, 1851–1866. [https://doi.org/10.1175/JHM-D-](https://doi.org/10.1175/JHM-D-18-0206.1)
474 [18-0206.1](https://doi.org/10.1175/JHM-D-18-0206.1)

475 Bahadur, R., Samuels, W.B., 2013. Application of Remote Sensing and Satellite Imagery for Hydrologic
476 Modeling [WWW Document]. *Environ. Water Resour. Inst.* URL
477 [http://message.asce.org/LP=205?utm_campaign=EWRI-20130429-](http://message.asce.org/LP=205?utm_campaign=EWRI-20130429-EWRI+Currents+Spring+2013&utm_medium=email)
478 [EWRI+Currents+Spring+2013&utm_medium=email](http://message.asce.org/LP=205?utm_campaign=EWRI-20130429-EWRI+Currents+Spring+2013&utm_medium=email) (accessed 1.17.21).

479 Bjerklie, D.M., Birkett, C.M., Jones, J.W., Carabajal, C., Rover, J.A., Fulton, J.W., Garambois, P.A., 2018.
480 Satellite remote sensing estimation of river discharge : Application to the Yukon River Alaska. *J.*
481 *Hydrol.* 561, 1000–1018. <https://doi.org/10.1016/j.jhydrol.2018.04.005>

482 Bjerklie, D.M., Dingman, S.L., Vorosmarty, C.J., Bolster, C.H., Congalton, R.G., 2003. Evaluating the
483 potential for measuring river discharge from space 278, 17–38. [https://doi.org/10.1016/S0022-](https://doi.org/10.1016/S0022-1694(03)00129-X)
484 [1694\(03\)00129-X](https://doi.org/10.1016/S0022-1694(03)00129-X)

485 Bjerklie, D.M., Moller, D., Smith, L.C., Dingman, S.L., 2005. Estimating discharge in rivers using remotely
486 sensed hydraulic information. *J. Hydrol.* 309, 191–209. <https://doi.org/10.1016/j.jhydrol.2004.11.022>

487 Bogning, S., Frappart, F., Blarel, F., Niño, F., Mahé, G., Bricquet, J.P., Seyler, F., Onguéné, R., Etamé, J.,

488 Paiz, M.C., Braun, J.J., 2018. Monitoring water levels and discharges using radar altimetry in an
489 ungauged river basin: The case of the Ogooué. *Remote Sens.* 10. <https://doi.org/10.3390/rs10020350>

490 Brasil/ANA, 2015. Conjuntura dos recursos hídricos no Brasil: regiões hidrográficas brasileiras.

491 Cooley, S.W., Smith, L.C., Ryan, J.C., Pitcher, L.H., Pavelsky, T.M., 2019. Arctic-Boreal Lake Dynamics
492 Revealed Using CubeSat Imagery. *Geophys. Res. Lett.* 46, 2111–2120.
493 <https://doi.org/10.1029/2018GL081584>

494 Cooley, S.W., Smith, L.C., Stepan, L., Mascaro, J., 2017. Tracking dynamic northern surface water changes
495 with high-frequency planet CubeSat imagery. *Remote Sens.* 9, 1–21.
496 <https://doi.org/10.3390/rs9121306>

497 Dixon, H., Sandström, S., Cudennec, C., Lins, H.F., Abrate, T., Bérod, D., Chernov, I., Ravalitera, N.,
498 Sighomnou, D., Teichert, F., 2020. Intergovernmental cooperation for hydrometry—what, why and
499 how? *Hydrol. Sci. J.* 00, 1–15. <https://doi.org/10.1080/02626667.2020.1764569>

500 Döll, P., Jiménez-Cisneros, B., Oki, T., Arnell, N.W., Benito, G., Cogley, J.G., Jiang, T., Kundzewicz,
501 Z.W., Mwakalila, S., Nishijima, A., 2014. Integrating risks of climate change into water management.
502 *Hydrol. Sci. J.* 60, 4–13. <https://doi.org/10.1080/02626667.2014.967250>

503 Elshahi, M., Negm, A., Hamid M.H. El Tahan, A., 2016. Performances Evaluation of Surface Water Areas
504 Extraction Techniques Using Landsat ETM+ Data: Case Study Aswan High Dam Lake (AHDL).
505 *Procedia Technol.* 22, 1205–1212. <https://doi.org/10.1016/j.protcy.2016.02.001>

506 Gleason, C.J., Smith, L.C., 2014. Toward global mapping of river discharge using satellite images and at-
507 many-stations hydraulic geometry. *Proc. Natl. Acad. Sci. U. S. A.* 111, 4788–4791.
508 <https://doi.org/10.1073/pnas.1317606111>

509 Hannah, D.M., Demuth, S., van Lanen, H.A.J., Looser, U., Prudhomme, C., Rees, G., Stahl, K., Tallaksen,
510 L.M., 2011. Large-scale river flow archives: Importance, current status and future needs. *Hydrol.*
511 *Process.* 25, 1191–1200. <https://doi.org/10.1002/hyp.7794>

512 Houborg, R., McCabe, M.F., 2018a. A Cubesat enabled Spatio-Temporal Enhancement Method
513 (CESTEM) utilizing Planet, Landsat and MODIS data. *Remote Sens. Environ.* 209, 211–226.
514 <https://doi.org/10.1016/j.rse.2018.02.067>

515 Houborg, R., McCabe, M.F., 2018b. Daily retrieval of NDVI and LAI at 3 m resolution via the fusion of
516 CubeSat, Landsat, and MODIS data. *Remote Sens.* 10. <https://doi.org/10.3390/rs10060890>

517 Huang, C., Chen, Y., Zhang, S., Wu, J., 2018. Detecting, Extracting, and Monitoring Surface Water From

518 Space Using Optical Sensors: A Review. *Rev. Geophys.* 56, 333–360.
519 <https://doi.org/10.1029/2018RG000598>

520 Joshi, N., Baumann, M., Ehammer, A., Fensholt, R., Grogan, K., Hostert, P., Jepsen, M.R., Kuemmerle, T.,
521 Meyfroidt, P., Mitchard, E.T.A., Reiche, J., Ryan, C.M., 2016. A Review of the Application of
522 Optical and Radar Remote Sensing Data Fusion to Land Use Mapping and Monitoring 1–23.
523 <https://doi.org/10.3390/rs8010070>

524 Kääb, A., Altena, B., Mascaro, J., 2019. River-ice and water velocities using the Planet optical cubesat
525 constellation. *Hydrol. Earth Syst. Sci.* 23, 4233–4247. <https://doi.org/10.5194/hess-23-4233-2019>

526 Karpatne, A., Ebert-Uphoff, I., Ravela, S., Babaie, H.A., Kumar, V., 2019. Machine Learning for the
527 Geosciences: Challenges and Opportunities. *IEEE Trans. Knowl. Data Eng.* 31, 1544–1554.
528 <https://doi.org/10.1109/TKDE.2018.2861006>

529 Kingston, D.G., Massei, N., Dieppois, B., Hannah, D.M., Hartmann, A., Lavers, D.A., Vidal, J.P., 2020.
530 Moving beyond the catchment scale: Value and opportunities in large-scale hydrology to understand
531 our changing world. *Hydrol. Process.* 34, 2292–2298. <https://doi.org/10.1002/hyp.13729>

532 Lakshmi, V., 2004. Use of Satellite Remote Sensing in, in: *International Journal*. Istanbul.

533 Latrubesse, E.M., Stevaux, J.C., 2006. Características físico-bióticas e problemas ambientais associados à
534 planície aluvial do Rio Araguaia - Brasil Central. *Rev. UnG - Geociências* 5, 65–73.

535 Lauris, P., 2019. Comitê pede ao Naturatins a suspensão das outorgas de captação de água na Bacia do Rio
536 Formoso [WWW Document]. *J. do Tocantins*. URL
537 [https://www.jornaldotocantins.com.br/editorias/vida-urbana/comitê-pede-ao-naturatins-a-](https://www.jornaldotocantins.com.br/editorias/vida-urbana/comitê-pede-ao-naturatins-a-suspensão-das-outorgas-de-captação-de-água-na-bacia-do-rio-formoso-1.1875921)
538 [suspensão-das-outorgas-de-captação-de-água-na-bacia-do-rio-formoso-1.1875921](https://www.jornaldotocantins.com.br/editorias/vida-urbana/comitê-pede-ao-naturatins-a-suspensão-das-outorgas-de-captação-de-água-na-bacia-do-rio-formoso-1.1875921) (accessed
539 2.14.20).

540 Lettenmaier, D.P., 2007. Measuring Surface Water From Space. *Rev. Geophys.* 45, 1–24.
541 <https://doi.org/10.1029/2006RG000197.1>.INTRODUCTION

542 Lettenmaier, D.P., Alsdorf, D., Dozier, J., Huffman, G.J., Pan, M., Wood, E.F., 2015. Inroads of remote
543 sensing into hydrologic science during the Water Resources Research era. *J. Am. Water Resour.*
544 *Assoc.* 5, 2–2. <https://doi.org/10.1111/j.1752-1688.1969.tb04897.x>

545 Maciel, D.A., Márcia, E., Moraes, L. De, Barbosa, C.F., Martins, V.S., Júnior, R.F., Oliveira, H., Augusto,
546 L., Carvalho, S. De, Lobo, F.D.L., 2020. Evaluating the potential of CubeSats for remote sensing
547 reflectance retrieval over inland waters. *Int. J. Remote Sens.* 41, 2807–2817.

548 <https://doi.org/10.1080/2150704X.2019.1697003>

549 Mannschatz, T., Wolf, T., Hülsmann, S., 2015. Nexus Tools Platform: Web-based comparison of
550 modelling tools for analysis of water-soil-waste nexus *Environmental Modelling & Software* Nexus
551 Tools Platform: Web-based comparison of modelling tools for analysis of water-soil-waste nexus.
552 *Environ. Model. Softw.* 76, 137–153. <https://doi.org/10.1016/j.envsoft.2015.10.031>

553 Mao, F., Clark, J., Buytaert, W., Krause, S., Hannah, D.M., 2018. Water sensor network applications: Time
554 to move beyond the technical? *Hydrol. Process.* 32, 2612–2615. <https://doi.org/10.1002/hyp.13179>

555 Mao, F., Khamis, K., Clark, J., Krause, S., Buytaert, W., Ochoa-Tocachi, B.F., Hannah, D.M., 2020.
556 Moving beyond the Technology: A Socio-technical Roadmap for Low-Cost Water Sensor Network
557 Applications. *Environ. Sci. Technol.* 54, 9145–9158. <https://doi.org/10.1021/acs.est.9b07125>

558 Mao, F., Khamis, K., Krause, S., Clark, J., Hannah, D.M., 2019. Low-Cost Environmental Sensor
559 Networks: Recent Advances and Future Directions. *Front. Earth Sci.*
560 <https://doi.org/10.3389/feart.2019.00221>

561 Marinho, C.S., Sacramento, V., Cangiano, M.R., Cicerelli, R.E., Almeida, T., 2020. Accumulated
562 Reflectance Technique for Sampling Delimitation in the Riacho Fundo Creek, Lago Paranoá-Df,
563 from Planetscope Images. 2020 IEEE Lat. Am. GRSS ISPRS Remote Sens. Conf. LAGIRS 2020 -
564 Proc. XLII, 259–263. <https://doi.org/10.1109/LAGIRS48042.2020.9165645>

565 Moramarco, T., Barbetta, S., Bjerklie, D.M., Fulton, J.W., Tarpanelli, A., 2019. River Bathymetry Estimate
566 and Discharge Assessment from Remote Sensing. *Water Resour. Res.* 55, 6692–6711.
567 <https://doi.org/10.1029/2018WR024220>

568 Mostafavi, M., 2018. River Monitoring Over Amazon and Danube Basin Using Multi- Mission Satellite
569 Radar Altimetry. *J. Hydrogeol. Hydrol. Eng. Res.* 7:2, 16. <https://doi.org/10.4172/2325-9647.1000167>

571 Musa, Z.N., Popescu, I., Mynett, A., 2015. C:\Users\adriano.junqueira\Documents\Adriano
572 2021\Doutorado\Artigos Acessados\2018 - A Review on Applications of Remote Sensing and
573 Geographic Information Systems (GIS) in Water Resources and Flood Risk Management.pdf for
574 surface water modelling, mapping . *Hydrol. Earth Syst. Sci.* 19, 3755–3769.
575 <https://doi.org/10.5194/hess-19-3755-2015>

576 Naturatins, 2017. Portaria Naturatins 300. Diário Of. do Estado do Tocantins - Bras. 45.

577 Norris, J.M., 2010. U . S . Geological Survey Streamgauge Operation and Maintenance Cost Evaluation (No.

578 Fact Sheet 2010-3025).

579 Planet Team, 2020. Planet Imagery Product Specifications - June 2020. San Francisco.

580 Pôssa, É.M., Maillard, P., Gomes, M.F., Silva, I., Leão, G., 2018. On water surface delineation in rivers
581 using Landsat-8, Sentinel-1 and Sentinel-2 data, in: SPIE Remote Sensing 2018 - Remote Sensing
582 for Agriculture, Ecosystems, and Hydrology. Berlin, p. 45. <https://doi.org/10.1117/12.2325725>

583 Reichle, R.H., 2008. Data assimilation methods in the Earth sciences. *Adv. Water Resour.* 31, 1411–1418.
584 <https://doi.org/10.1016/j.advwatres.2008.01.001>

585 Reichstein, M., Camps-Valls, G., Stevens, B., Jung, M., Denzler, J., Carvalhais, N., Prabhat, 2019. Deep
586 learning and process understanding for data-driven Earth system science. *Nature* 566, 195–204.
587 <https://doi.org/10.1038/s41586-019-0912-1>

588 Sadeh, Y., Zhu, X., Chenu, K., Dunkerley, D., 2019. Sowing date detection at the field scale using CubeSats
589 remote sensing. *Comput. Electron. Agric.* 157, 568–580.
590 <https://doi.org/10.1016/j.compag.2019.01.042>

591 Samboko, H.T., Abas, I., Luxemburg, W.M.J., Savenije, H.H.G., Makurira, H., Banda, K., Winsemius,
592 H.C., 2020. Evaluation and improvement of remote sensing-based methods for river flow
593 management. *Phys. Chem. Earth* 117, 102839. <https://doi.org/10.1016/j.pce.2020.102839>

594 Smith, L.C., Pavelsky, T.M., 2008. Estimation of river discharge , propagation speed , and hydraulic
595 geometry from space : Lena River , Siberia 44, 1–11. <https://doi.org/10.1029/2007WR006133>

596 Wagner, W., Lucieer, A., Houborg, R., Verhoest, N.E.C., 2018. The Future of Earth Observation in
597 Hydrology. *Hydrol Earth Syst Sci* 21, 3879–3914. <https://doi.org/10.5194/hess-21-3879-2017>.The

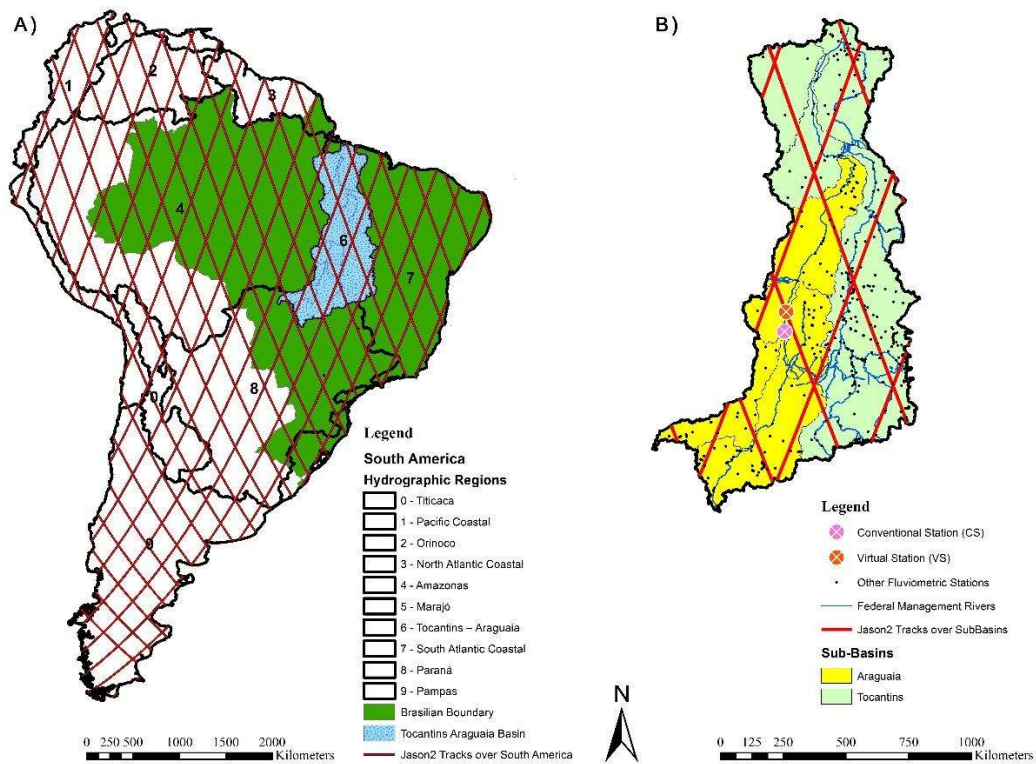
598 Zaji, A.H., Bonakdari, H., Gharabaghi, B., 2018. Remote Sensing Satellite Data Preparation for Simulating
599 and Forecasting River Discharge. *IEEE Trans. Geosci. Remote Sens.* 56, 3432–3441.
600 <https://doi.org/10.1109/TGRS.2018.2799901>

601

602 **Figures**

603

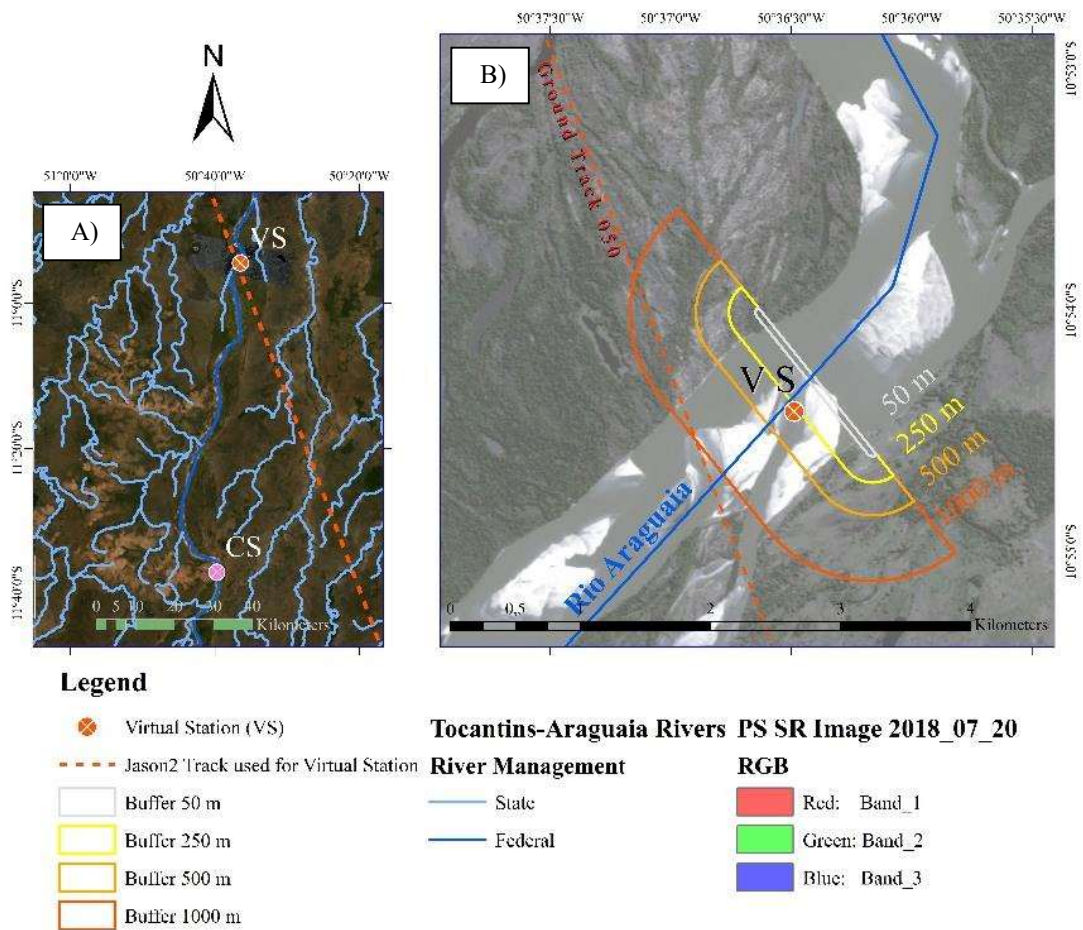
604 **Fig. 1.** Overview of the study area. (A) Overview of South America with its 10 Hydrographic Regions
605 (black), passes of JASON-2 over the area (red), and the Tocantins-Araguaia basin (light blue); (B) Zoom
606 in the Tocantins (light-green) - Araguaia (yellow) basin boundaries, presence of rivers with federal
607 regulation (blue) and all fluviometric in situ stations (black dots), complemented by tracks of Jason-2 (red)
608 highlighting JVS (red circle; north) and CS (pink circle; south) ground references.



609

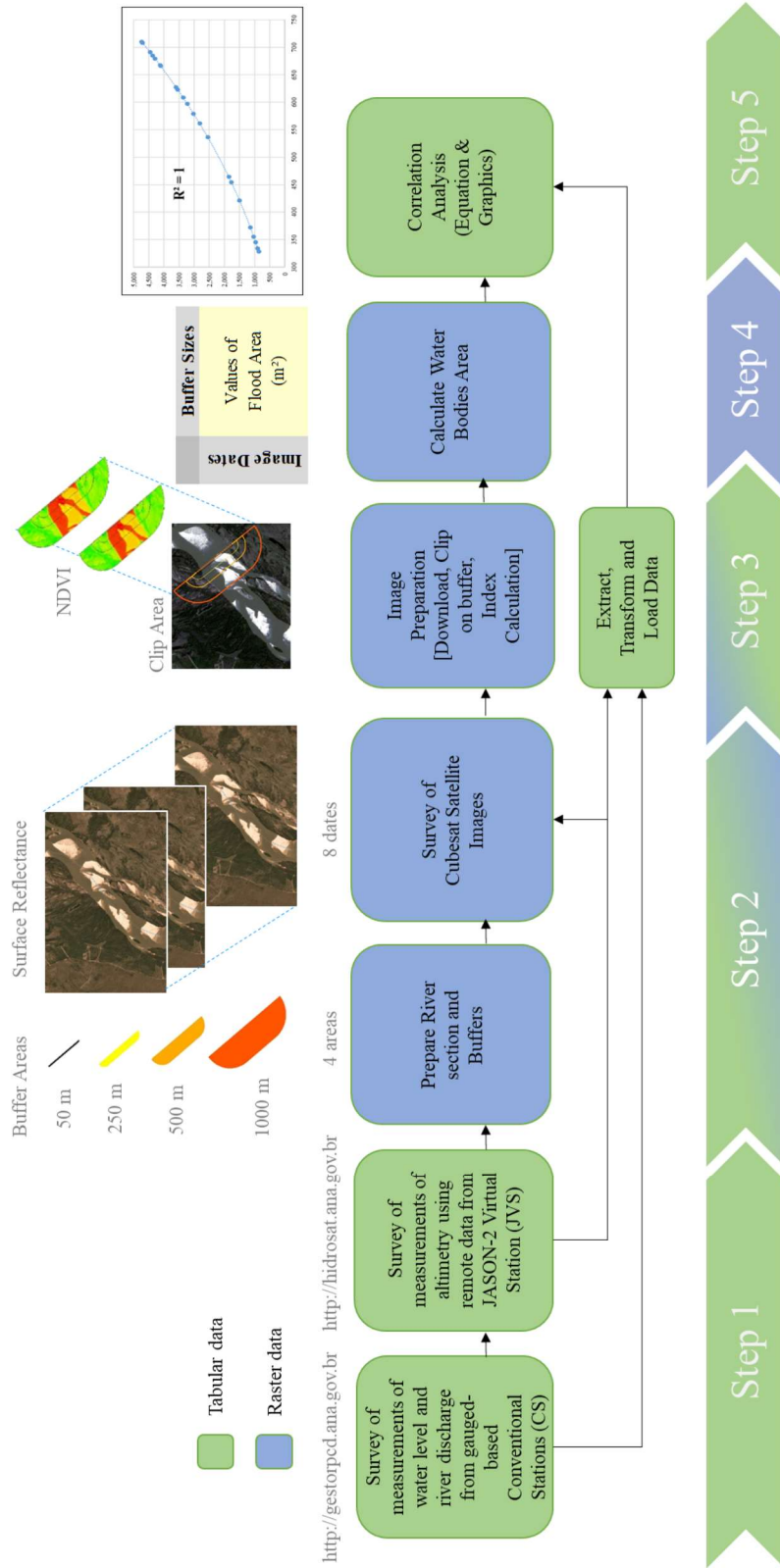
610

611 **Fig. 2.** The study area of the Araguaia sub-basin. (A) Zoom in the Araguaia River (center) highlighting the
 612 track of Jason-2 (red) over the surface drainage (blue), and the Conventional Station (CS) used as ground
 613 truth (pink dot). The region where the Jason-2 track crosses the Araguaia River is the Virtual Station (JVS)
 614 far 78 km from CS and, the region used to download the CubeSat SR images;
 615 over the Araguaia River (blue line) with the 4 different buffer areas used in the methodology (50 m – grey;
 616 250 m – yellow; 500 m – orange; 1000 m – red). In the background it is presented the Surface Reflectance
 617 (SR) Planet image from July, 20th 2018 with 50% transparency and the representation of the Jason-2 track
 618 over the region (red dashed line).
 619



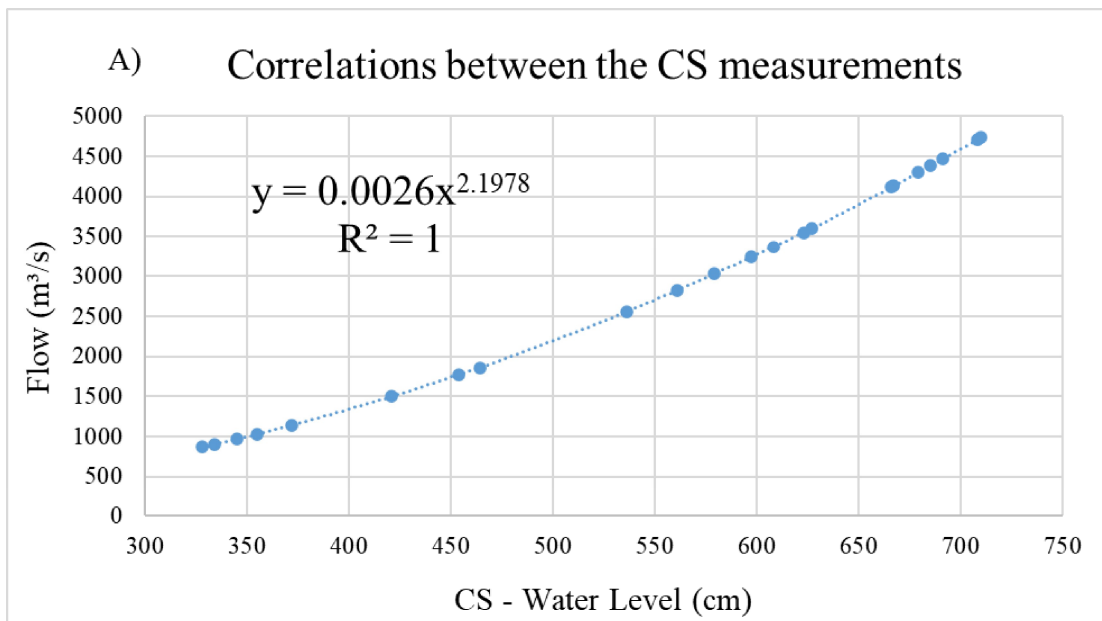
620
 621

622 **Fig. 3.** Methodological framework using CubeSat to estimate the river flow. The 1st step is used for
623 gathering reference information to support the key-curves. In the 2nd step are prepared the specific buffer
624 areas and selected the CubeSat images to investigate the correlation between inundation extent and river
625 flow. The 3rd step is used for preprocessing selected CubeSat images with pixel classification (water/no-
626 water) based on NDVI values. In the 4th step are calculated the flooding area for each image. The last step
627 is to evaluate the regression analysis comparing the 3 reference data (CS - Flow river; CS – Water Level;
628 JVS – Altimetry).



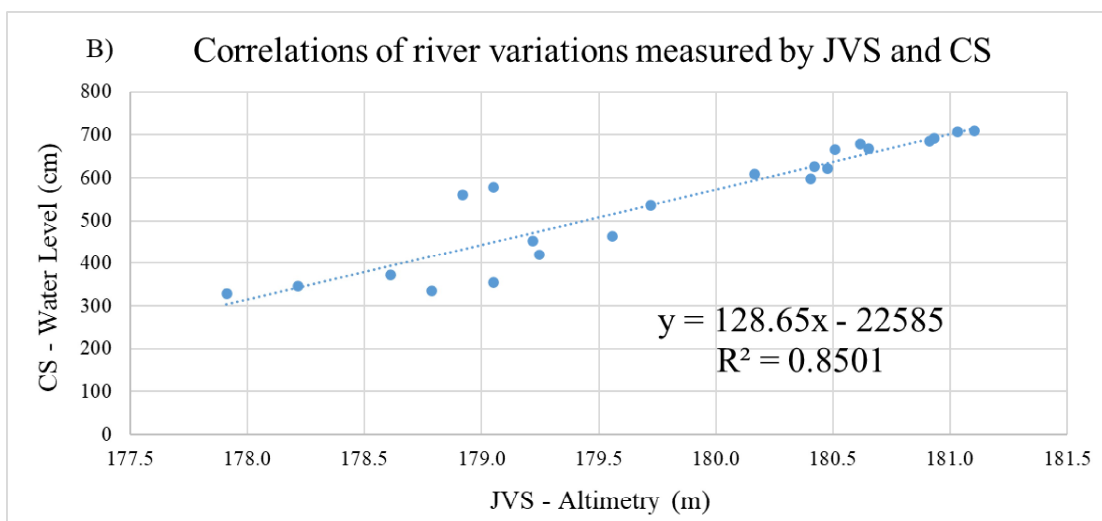
630 **Fig. 4.** Evaluation of the reference data. **(a)** Relationship between the river level (x-axis) and flow (y-axis)
 631 by the CS in the São Felix do Araguaia/MT station for the period of analyses. The blue curve represents
 632 the exponential equation ($y = 0.0026x^{2.1978}$) that are well adjusted with $R^2 = 1$.
 633 **(b)** Relationship between the altitudes (x-axis) calculated by the JVS and the quotes determined on the
 634 water level (y-axis) by the CS in the Araguaia basin for the period of analyses. The blue curve represents
 635 the linear equation ($y = 128.65x - 22585$) with $R^2 = 0.8501$. In both figures, the solid blue circles represent
 636 correlated values with 10 days interval.

637



638

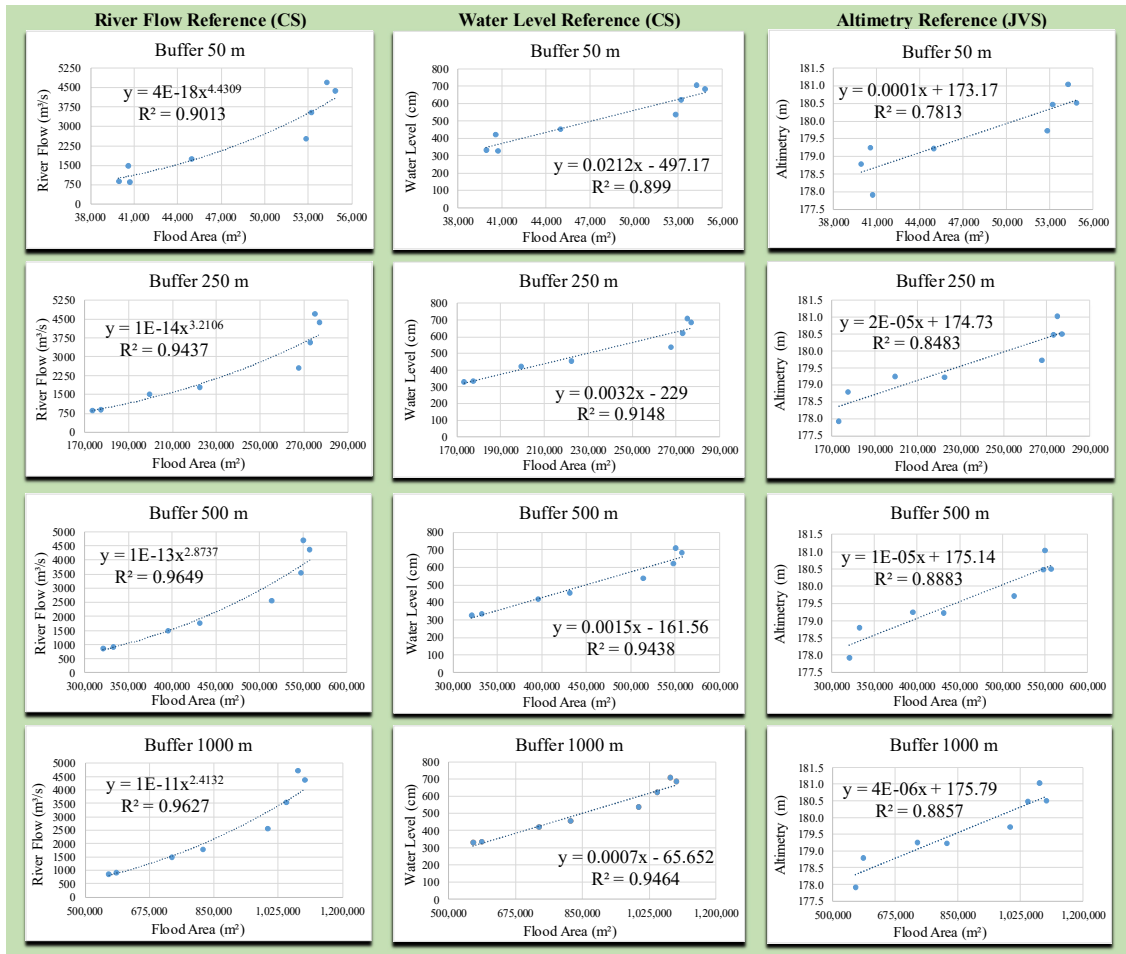
639



640

641 **Fig. 5.** Regression curves against 3 ground references and 4 different buffer sizes

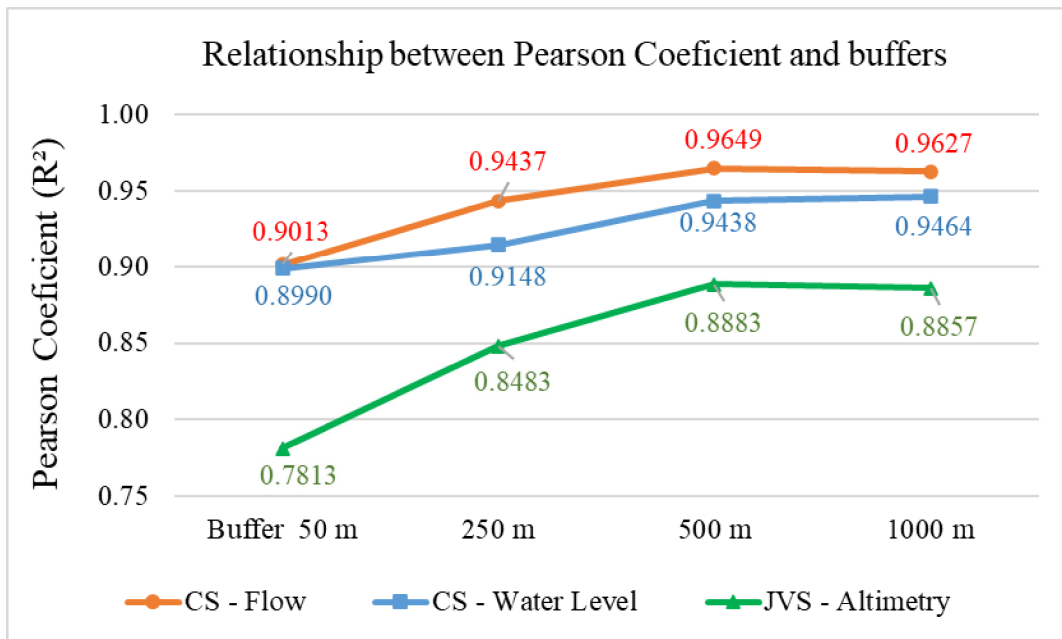
642



643

644

645 **Fig. 6.** Relationship between R^2 (x-axis) and 4 buffers distances (y-axis) for 3 sets of reference data (CS
646 water level and river flow and JVS altimetry).
647



648
649

650 **Tables**

651

652 **Table 1.** Detail of measurements related to JVS, CS, and satellite images used in the period of analysis
 653 for river flow estimates.

654

Label ID	Date	JASON	Conventional	Conventional	Surface Reflectance
		Virtual Station (JVS) Altimetry (m)	Station (CS) Water Level (cm)	Station (CS) River Flow (m ³ /s)	(SR) Planet CubeSat Images
1	2018 01 03	179.049	579	3,022.10	incomplete/cloud
2	2018 01 13	178.917	561	2,819.00	incomplete/cloud
3	2018 01 23	180.478	623	3,551.62	available
4	2018 02 02	180.404	597	3,233.03	incomplete/cloud
5	2018 02 12	180.165	608	3,365.81	incomplete/cloud
6	2018 02 22	180.615	679	4,294.38	incomplete/cloud
7	2018 03 04	181.030	708	4,709.77	available
8	2018 03 13	181.103	710	4,739.20	incomplete/cloud
9	2018 03 23	180.913	685	4,378.59	incomplete/cloud
10	2018 04 02	180.931	691	4,463.70	incomplete/cloud
11	2018 04 12	180.651	667	4,128.66	incomplete/cloud
12	2018 04 22	180.508	666	4,115.01	available
13	2018 05 02	180.419	627	3,602.11	incomplete/cloud
14	2018 05 12	179.721	536	2,549.77	available
15	2018 05 22	179.557	464	1,856.67	TOA image
16	2018 06 01	179.220	454*	1,769.96*	available
17	2018 06 11	179.248	421	1,499.74	available
18	2018 06 21	178.612	372	1,143.57	TOA image

19	2018 07 01	179.049	355	1,032.33	incomplete/cloud
20	2018 07 10	178.217	345	969.81	incomplete/cloud
21	2018 07 20	178.786	334	903.52	available
22	2018 07 30	177.912	328	868.46	available

* average between 02/06/2018 and 31/05/2018

655

Label ID	Date	JASON	Conventional	Conventional	Surface Reflectance
		Virtual Station (JVS) Altimetry (m)	Station (CS) Water Level (cm)	Station (CS) River Flow (m ³ /s)	(SR) Planet CubeSat Images
1	2018 01 03	179.049	579	3,022.10	incomplete/cloud
2	2018 01 13	178.917	561	2,819.00	incomplete/cloud
3	2018 01 23	180.478	623	3,551.62	available
4	2018 02 02	180.404	597	3,233.03	incomplete/cloud
5	2018 02 12	180.165	608	3,365.81	incomplete/cloud
6	2018 02 22	180.615	679	4,294.38	incomplete/cloud
7	2018 03 04	181.030	708	4,709.77	available
8	2018 03 13	181.103	710	4,739.20	incomplete/cloud
9	2018 03 23	180.913	685	4,378.59	incomplete/cloud
10	2018 04 02	180.931	691	4,463.70	incomplete/cloud
11	2018 04 12	180.651	667	4,128.66	incomplete/cloud
12	2018 04 22	180.508	666	4,115.01	available
13	2018 05 02	180.419	627	3,602.11	incomplete/cloud
14	2018 05 12	179.721	536	2,549.77	available
15	2018 05 22	179.557	464	1,856.67	TOA image
16	2018 06 01	179.220	454*	1,769.96*	available
17	2018 06 11	179.248	421	1,499.74	available
18	2018 06 21	178.612	372	1,143.57	TOA image
19	2018 07 01	179.049	355	1,032.33	incomplete/cloud
20	2018 07 10	178.217	345	969.81	incomplete/cloud
21	2018 07 20	178.786	334	903.52	available
22	2018 07 30	177.912	328	868.46	available

* average between 02/06/2018 and 31/05/2018

656

657 **Table 2.** Flood area calculated inside buffers with NDVI value smaller than 0.15.

658

Label ID	Selected dates of Surface Reflectance (SR) Planet CubeSat Images	Flood Area	Flood Area	Flood Area	Flood Area
		inside Buffer 50m (m ²)	inside Buffer 250m (m ²)	inside Buffer 500m (m ²)	inside Buffer 1000m (m ²)
3	2018 01 23	53,181	273,024	547,929	1,046,745
7	2018 03 04	54,261	275,040	550,251	1,079,640
12	2018 04 22	54,846	276,984	557,586	1,097,469
14	2018 05 12	52,839	267,615	513,891	997,580
16	2018 06 01	44,964	222,336	431,730	819,477
17	2018 06 11	40,572	199,512	395,604	736,335
21	2018 07 20	39,924	177,471	332,415	585,909
22	2018 07 30	40,707	173,313	320,805	563,895

659

660 **Table 3.** Accuracy (*RMSE*) and precision (*SD*) estimators related to river flow (*Qe*), water level (*Le*) and
 661 altimetry (*Ae*)
 662

Regression Curves	Accuracy Estimator (<i>RMSE</i>)	Precision Estimator (<i>SD</i>)	Unit
River Flow (<i>Qe</i>)	717.59	553.63	m ³ /s
Water Level (<i>Le</i>)	59.45	37.16	cm
Altimetry (<i>Ae</i>)	0.33	0.34	m

663